ACS OMEGA

Open Access

http://pubs.acs.org/journal/acsodf

Article

Fabrication of Supported and Unsupported Gold Nanorods for Nonenzymatic Glucose Sensing and Study of Their Growth Kinetics

Sana Sabahat,* Yumna Nazish, Farhat Saira, Iqra Tariq, Zia Ul Haq Khan, Rahman Shah Zaib Saleem, Mahmood M. S. Abdullah, and Yong-Mei Chen

Cite This: *ACS Omega* 2024, 9, 33616−33628

Read Online

ACCESS | Metrics & More | Article Recommendations | Supporting Information

ABSTRACT: This work includes a novel approach for synthesis/fabrication of AuNRs of varied aspect ratios leading to investigation on the kinetics of their growth mechanism. The synthesized AuNRs were further functionalized with MWCNTs (AuNRs@MWCNTs) by one-pot synthesis. The synthesized AuNRs and AuNRs@MWCNTs were characterized by employing UV−vis spectroscopy. Red shifts in the spectra of AuNRs confirmed the formation of nanorods of higher aspect ratios. Morphology of AuNRs and functionalized AuNRs was confirmed by high-resolution scanning electron microscopy. Biological studies were carried out by fabricating efficient nonenzymatic glucose sensors for optical and electrochemical sensing via UV and cyclic voltammetry in the detection ranges of 0.7−28 mM glucose (UV) and 5.5 μM−0.33 mM (CV). An electrochemical sensing study was carried out via AuNR- and AuNRs@MWCNT-modified GCEs in a 0.1 M NaOH electrolyte solution. The modified electrodes exhibited very high sensitivity with a broad linear range. The order of sensitivity (via CV) was found to be $AuNRX_0$@MWCNTs > $AuNRD_5$@MWCNTs > $AuNRD_5$ > $AuNRX_0$.

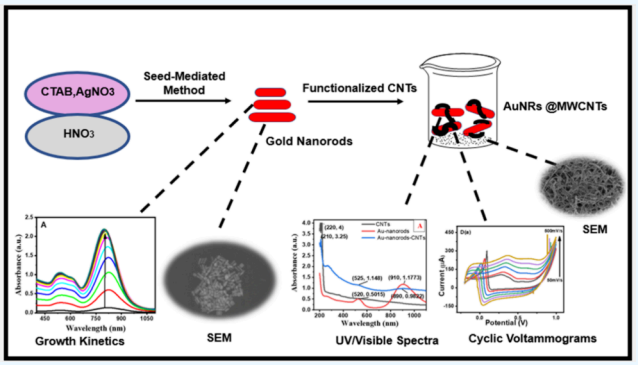

RESEARCH HIGHLIGHTS

- Synthesis of AuNRs of different aspect ratio for sensing applications
- Fabrication of AuNRs@MWCNTs via one-pot synthetic method
- Electrocatalysis and catalytic investigations of AuNRs and AuNRs@MWCNTs
- Nonenzymatic glucose sensing via AuNRs and AuNRs@MWCNTs
- Study of growth kinetics of AuNRs

1. INTRODUCTION

Nanomaterials denote a highly varied class of materials whose structural constituents have dimensions not exceeding 100 nm in at least one of the dimensions. This class of material has a very high surface area-to-volume ratio. Its intrinsic properties at the nanoscale are profoundly linked to both the arrangement and the quantity of surface atoms.[1]

The fundamental properties of matter transform at the nanoscale, and nanomaterials have manifested interesting and valuable properties. Nanoparticles' physical and chemical characteristics can differ significantly from those of the same substance's larger particles. In contrast to bulk materials, they are comparable in size than single atoms and particles; hence, it is imperative to apply quantum mechanics to understand how they function.[2] When compared to their bulk equivalents, nanoparticles have distinctive optical, electrical, magnetic, and thermodynamic properties. The electrical, mechanical, magnetic, and optical properties of nanostructures are highly susceptible by anisotropy at the nanoscale.[3] Owing to the spatial confinement, electrons' mobility affects both their chemical and physical properties. For relatively small nanoparticles, the surface atom's coordination number is lower than its internal atoms, permitting the electron to move freely. When evaluating a nanomaterial's properties, shape and size matter. Particles exhibit quantum size effects when their size is close to the limit of the de Broglie wavelength, and their diameter is less than that of the interaction between quasiparticles. Materials based on surface traits (such as surface area or surface tension) can be used in nanoelectronics, catalysis, adsorption, sensors, and functional coatings. Their properties rely on their size including emission, extinction, stability, and chemical reactivity.

Noble metal nanoparticle-CNT composites, in which the nanoparticles are bonded to a surface of the CNTs, have potential uses in sensing, optical electronics, including

Received: February 19, 2024
Revised: July 1, 2024
Accepted: July 12, 2024
Published: July 24, 2024

heterogeneous catalysis because of extremely large specific area, electrical properties, and distinctive structural features.[4] Gold- and silver-coated CNTs also improve broad-band optical limiters.[5] Potential uses for the AuNPs@CNT system included an amperometric acetylcholinesterase biosensor and a nanostructure-based DNA sensor.[6] In an aqueous solution, 1-pyrenemethylamine served as the bridge to produce Au. In organic media, composites of metal nanoparticles and carbon nanotubes have been developed and characterized. In organic media, nanotube nanoparticle composites were created and characterized. Silver nanoparticles were added to carbon nanotubes to develop advanced CNT/polymer nanocomposites.[7] AuNPs may be loaded onto CNTs through regenerative ion exchange, as well. Multiwalled carbon nanotubes that have been functionalized are used to create these AuNPs@CNT nanocomposites.[8] These findings demonstrate that a wide range of potential applications are provided by the high-density and homogeneous assembly of AuNPs on CNTs.

Gold nanorods among nonspherical nanomaterials have length-to-diameter aspect ratios larger than 1, but less than 10, and their usual length extends from a few nanometers over hundreds of nanometers. Due to their particular physical properties, the exceptional physical and chemical properties of gold nanorods, such as optical,[9] electronic,[10] magnetic,[11] and catalytic[12] nanorods, have versatile applications in a variety of industries, such as medical,[13] bioscience,[14] electronic,[10] mechanical technologies,[15] sensors,[16] and solar cells,[17] which have promoted their potential uses in different areas of chemistry, physics, biology, medicine, and much more others. The discrete properties and extraordinary applications of nanomaterials are dependent on their size, surface morphology, and inter particle interactions. Nanorods absorb primary light, and Au exhibits a localized surface plasmon resonance (LSPR) in the visible range between 700 and 900 nm and a surface plasmon resonance (SPR) band at 520 nm. The LSPR splits into two different plasmon modes to demonstrate the optical characteristics of the rods. Light scattering rises with increasing aspect ratio of nanorods, which causes a shift toward longer wavelengths and broadens the peaks/band and intensity. As the length and breadth of nanorods increase, shifts of longitudinal band toward higher wavelength (aspect ratio) occur.[18]

The seed-mediated technique is in situ synthesis, which isolates seed production and development as distinct synthetic phases and enables rational design of nanomaterials with various shapes and sizes by selecting a particular seed as well as binding surfactants. In a conventional seed-mediated technique, the whole creation process typically entails three steps: (1) nucleation, (2) nuclei to seeds evolution, and (3) seeds to nanorods evolution.[19] The first two stages are related to seed formulation. The tiny particles that initially caused the nucleation into gold atoms are known as the "seed". The seed is thought to be a sturdy, faceted structure that plays a significant role in guiding the development and evolution of further structures. Because of its ease of use, high yield, and adaptability to changes, the seed-mediated approach is being used for the fabrication of gold nanomaterials with tunable shapes and sizes. Noble metal-supported nanomaterial-MWCNT composites have potential applications in sensing, optical electronics, and heterogeneous catalysis because of availability of large surface areas and distinctive structural features.[20,21] Different synthetic protocols have been adopted for the synthesis of gold nanomaterial-decorated @MWCNTs.[22,23] Chinh et al. reported gold nanoparticle-decorated multiwalled carbon nanotubes (MWCNTs) adopting cysteaminium chloride via the formation of a zwitterionic acid−base bond.[24]

Glucose is the most essential biomolecule found in the human body; any abnormality in its concentration can have adverse effects on the functioning of the human body. The measurement of glucose content has significant relevance because of the direct impact on the biological system. It is frequently of interest to build a straightforward, affordable, direct, and real-time technique to monitor glucose levels. Therefore, for the prevention, diagnosis, and treatment of diabetes, glucose levels must be detected and monitored. Enzymes were used in the development of several glucose sensors to achieve great sensitivity and superior selectivity. However, the activity of the enzymes has a significant impact on the sensitivity, selectivity, and durability of enzyme-based glucose sensors.[25] The glucose enzyme's activity is influenced by the pH, humidity, and temperature.[26] Nonenzymatic sensors mostly have facile synthetic processes and inexpensive fabrication costs. When compared to enzymatic ones, they also have the advantages of greater sensitivity, selectivity, and stability.[27] Nanomaterials have played a vital role in detection of glucose[28−30] for which electrochemical and photoluminescence probes have been fabricated.[31−33] Gold nanorods have versatile applications because of their biocompatibility, noncytotoxicity, and enhanced optical, electrical, and magnetic characteristics.[34] Moreover, AuNRs incorporated onto MWCNTs by the regenerative ion method[35] have demonstrated versatile potential applications due to their high-density and homogeneous assembling as well as synergistic effect of both nanomaterials. As redox catalysts, gold nanoparticles may act as mediators for electrochemical processes, link to electrode surfaces, and enhance signals for bioprocessing. They are also helpful as electrochemical biosensors.[36] There have been several reports of electrochemical bioassay research using gold nanomaterials.[37,38] The use of gold nanorods has two major applications: bioassay nanoelectrodes[39] and biomolecular tracers.

In this work, a seed-mediated synthetic protocol was adopted for the preparation of LSPR-based gold nanorods for sensing applications. By variation of the amount of nitric acid, gold nanorods of varied aspect ratios were obtained. The fabrication of supported AuNRs@MWCNTs was done by adopting a one-pot facile method for sensing applications. The optical biosensing tool was optimized using UV−visible spectroscopy by modifying the previously reported method.[40] Electrochemical sensing of glucose was monitored via undecorated and decorated gold nanorods@MWCNTs.

Several research groups reported fabrication of nanomaterials with MWCNTs, and all of the studied methods are complex and slightly difficult. The novelty of our work is the presentation of a simple, facile, and one-pot synthetic protocol for fabrication of AuNRs@MWCNTs for nonenzymatic glucose sensing. The proposed strategy for AuNRs@MWCNTs has still not been reported. We also comprehensively discussed the growth kinetics of synthesized gold nanorods.

2. EXPERIMENTATION

2.1. Chemicals and Reagents. The chemicals and reagents used in this study were gold(III) chloride trihydrate ($HAuCl_4$), 99.9% purity from Sigma-Aldrich; cetyltrimethylammonium bromide (CTAB), 99.0% purity from Sigma-Aldrich; sodium borohydride ($NaBH_4$), 98.0% purity from Sigma-Aldrich; L-(+)-ascorbic acid (AA), 99.0% purity from Alfa Aesar; silver nitrate ($AgNO_3$), 99.9% purity from Alfa Aesar; nitric acid

https://doi.org/10.1021/acsomega.4c01313
ACS Omega 2024, 9, 33616−33628

Table 1. Summary of the Sample Codes Based on the Composition Used

sample	composition	
Au = gold, NR = nanorods	HNO_3 (μL)	pH
$AuNRX_0$	X_0 = 0 μL	3.13
$AuNRB_1$	B_1 = 100 μL	2.54
$AuNRC_2$	C_2 = 300 μL	1.96
$AuNRC_3$	C_3 = 400 μL	1.83
$AuNRB_3$	B_3 = 500 μL	1.70
$AuNRD_1$	D_1 = 600 μL	1.66
$AuNRD_2$	D_2 = 700 μL	1.64
$AuNRD_4$	D_4 = 900 μL	1.49
$AuNRD_5$	D_5 = 1100 μL	1.41
$AuNRX_0$ @MWCNTs	X_0 = 0 μL	
$AuNRD_5$ @MWCNTs	D_5 = 1100 μL	

(HNO_3), 69.9% purity from Sigma-Aldrich; D-glucose; multiwalled CNTs; aqua regia (HCl−HNO_3 3:1), and deionized water (DI). All glassware was cleaned with aqua regia before use to remove any contamination.

2.2. Synthesis of AuNRs. A modified seed-mediated method was adopted for the synthesis of the AuNRs.[41] During the synthesis process, in aqueous CTAB solution, the addition of gold salt turned the clear solution yellowish. 5 mL of 0.1 M CTAB was uniformly mixed with 55 μL of 0.025 M $HAuCl_4$ followed by the addition of 225 μL of ice-cold 0.025 M $NaBH_4$. The prepared solution was rested for 2 h before further use at a stable temperature of about 30 °C. For the preparation of growth solution, CTAB solution was prepared and an optimized amount of $HAuCl_4$ was added to CTAB. The colorless solution turned yellowish. $AgNO_3$ was added followed by addition of different amounts of nitric acid (0, 100, 300, 400, 500, 600, 700, 900, and 1100 μL) (Table 1). The addition of $AgNO_3$ and nitric acid is favorable for the growth of gold nanorods, whereas NO_3^{-1} plays a key role in the formation of high aspect ratio gold nanorods.[42−44] Ascorbic acid was then added in each vial, which turned the yellowish solution into a colorless solution. The disappearance of color when A.A was added is due to the reduction of Au^{3+} to Au^{+}. Ascorbic acid is a weak reducing agent; upon addition of seed solution, reduction of metal salt occurs as the color of solution rapidly changed.[45,46] Seeds were introduced in each solution and left the solutions undisturbed overnight on a hot plate at 30 °C.

2.3. Functionalization of MWCNTs. MWCNTs were pretreated with a mixture of HNO_3 and H_2SO_4 in a ratio of 1:3. For pretreatment, 0.5 g of MWCNTs was mixed with acid solutions and ultrasonicated for 6 h with intervals of 30 and 20 min of rest, keeping the temperature low. Then, the sonicated mixture was subjected for filtration until the pH of the solution became neutral at 7. The obtained mixture was allowed to evaporate in an oven at 80 °C. The dried sample was ground with mortar and pestle to obtain the fine powder. The functionalized MWCNTs were used for further experimentation.

2.4. Incorporation of AuNRs @MWCNTs. Functionalized MWCNTs were dispersed in deionized water (DI H_2O) at 1 mg/mL by using sonication. The sonication was performed for 30 s. The dispersion was mixed with 1 mL of colloidal Au nanorods. After shaking, the mixture was left at room temperature for 10 min. The decrease in color of the supernatant indicated the adsorption of AuNRs onto MWCNTs.

2.5. Materials Characterization. UV−visible spectroscopy (K-Lab OPTIZEN Alpha UV−vis spectrophotometer) was performed to study the stability and formation of supported and unsupported gold nanorods. Scanning electron microscopy (FEI Nova 450 NanoSEM) was carried out to investigate the morphology of the synthesized materials. The growth kinetics and optical glucose sensing of synthesized materials were studied via UV−visible spectroscopy. Electrochemical investigations (glucose sensing) via cyclic voltammetry (CV) were performed with a Gamry instrument.

2.6. Direct Optical and Electrochemical Sensing of Glucose via AuNRs. For direct optical sensing, 1 mL of the prepared gold nanorods (of different aspect ratios) was added to a series of 1.5 mL Eppendorf tubes containing glucose solution. 5 mL of each 0.1 M glucose concentration was added into a separate Eppendorf tube, and all tubes were placed in a sonicator at 30 °C for a duration of 5 min before the record of spectra. Electrochemical sensing was performed via CV with a Gamry potentiostat attached to Gamry software for integration. The temperature of 25 °C was maintained during all the experiments. 0.1 M solution of sodium hydroxide was used as a supporting electrolyte. The standard three-electrode system was employed in this experiment. Glassy carbon electrode (GCE) was used as the working electrode. Silver−silver chloride (Ag/AgCl) electrode was used as the reference electrode, and all the potential was referred to this electrode. The auxiliary electrode in this experiment was a platinum (Pt) wire. Modification of all the electrode assemblies was done carefully by combining reference and auxiliary electrodes and using a modified working electrode separately.

2.7. Modification of Electrode for Electrochemical Measurements. GCE was polished using polishing pads and alumina powder rinsed with deionized water followed by ultrasonication for 1 min in deionized water to eliminate alumina particles. At room temperature, all of the electrodes were dried. Cleaned and dried GCE was spotted with 5.0 μL of the synthesized samples. The electrodes were kept for 30 min for dryness in the air. These ready electrodes were used to investigate electrochemical performance. Prior to investigating the performance of modified electrodes, the bare electrode was scanned in 0.1 M NaOH.

3. RESULTS AND DISCUSSION

3.1. UV−Visible Spectroscopic Analysis. Figure 1 shows the UV spectra of the synthesized samples. Two characteristic peaks were observed in each case. Transverse surface plasmon resonance (TSPR) absorption bands at around 510−530 nm and longitudinal LLSPR absorption bands within 650 to 930 nm were observed. This confirms the formation of gold nanorods. The bathochromic shift with respect to increasing HNO_3 concentrations inferred that gold nanorods with different aspect ratios have been synthesized successfully.

3.2. Morphological Analysis via SEM. Figure 2a,b shows SEM images of gold nanorods without and with the maximum concentration of HNO_3. Figure 2b infers a uniform high-density packing arrangement of long gold nanorods with the addition of HNO_3. These synthesized gold nanorods were found straight, elongated, and uniform in dimensions.

3.3. Growth Kinetics Investigation via UV−Visible Spectroscopy. The reaction process of growing gold nanorods was monitored by recording the optical spectra of the plasmons. As studied, in the presence of a weak reducing agent, reduction of gold cannot be done completely from Au(III) ions to Au(0).

https://doi.org/10.1021/acsomega.4c01313
ACS Omega 2024, 9, 33616−33628

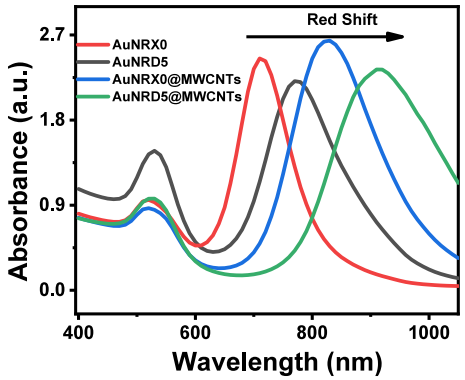

Figure 1. UV spectra of Au nanorods of varied aspect ratios. Bathochromic shift toward higher wavelength corresponding to increasing nitric acid concentration in AuNR synthesis.

At lower pH, there was a slow reduction of Au(III) to Au(I). Further addition of seeds resulted in reduction of Au(I) to Au(0), giving it a deposition room on the facets of spherical seed nanoparticles.[47] Since a minimal change in the pH of the growth solution is likely not the valid reason for the noticeable increase in the fabrication of long nanorods, the presence of nitrate ions on nanorod synthesis was therefore investigated. At lower pH, the weak reducing potential of ascorbic acid resulted in a slow reduction of Au and an increased repulsion between AuNRs due to the high concentration of H^+ in the solution that facilitated the growth of AuNRs of higher aspect ratio. It was found that nitrate ions, rather than the slight pH change produced with the introduction of nitric acid, exerted a greater influence on the formation of high aspect ratio nanorods. This is in accordance with the previously reported work.[48] It can also be proposed that with the addition of more nitric acid, there is more availability of nitrate ions, which enhanced self-assemblage as well as uniform high-density packing of gold nanorods. We believe that our study could provide a general and facile approach for the pH-sensitive synthesis of gold nanorods. The growth mechanism is displayed in the Supporting Information, Figure S1.

Experimental results were acquired every 150 s during 1.5 h, inferring the effect of the mechanism of pH on the size and morphology of gold nanorods. The higher pH favored the formation of smaller spherical or ellipsoidal nanoparticles, while a decrease in pH resulted in longer nanorods. During the AuNRs' growth process, the color changes of growth solution were faster as well as prominent at higher pH than at lower pH. For further investigation of the dynamic mechanism of AuNR synthesis, UV−vis spectra of the reaction solution during the growth of AuNRs were recorded. Figure 3 shows the LLSPR peak position of the solution as a function of the growth solution at pH of 3.13, 1.96, 1.70, and 1.41.

It can be seen in Figure 3A that at pH 3.13, for the original growth solution without adding HNO_3, the LLSPR peak appeared in 1 or 2 min. It red-shifted initially and then blue-shifted to 780 nm as the rods developed over time. However, at pH 1.41 in Figure 3D, the LLSPR peak was not visible at the start of the reaction, but after about 10 min, it increased and red-shifted gradually and then the growth rate slowed down after the saturation was attained.

3.4. Stages of the Growth Process. During the growth process, several stages were observed. At stage I, all seeds grew isotropically until a critical size was reached, which defined the transition to stage II. The transition to stage II for these seeds reflected a balance between the stabilization of adsorbed CTAB and the formation of a sufficiently large particle surface (Figure 4). Furthermore, the particles grew anisotropically, inferring that the growth took place faster on the exposed surface at the bottom and top of the rod.[49] Thus, the growth resulted to an increased aspect ratio leading in an evident red shift of the LLSPR.[50]

3.5. Statistical Analysis of the Growth Mechanism. The experimental data was fitted with theoretical nonlinear Boltzmann function, and normalized growth curves were plotted against time. For comparing the growth rates of reaction under acidic conditions, absorbance−time graphs were plotted, as displayed in Figure 5.

For the quantification of nanorod growth, maximum rates were obtained by fitting the data with the Boltzmann sigmoid[51,52] using the following equation:

$$\gamma = \frac{A_1 - A_2}{1 +_{\varepsilon} (x - x_0)/\mathrm{d}x} + A_2$$

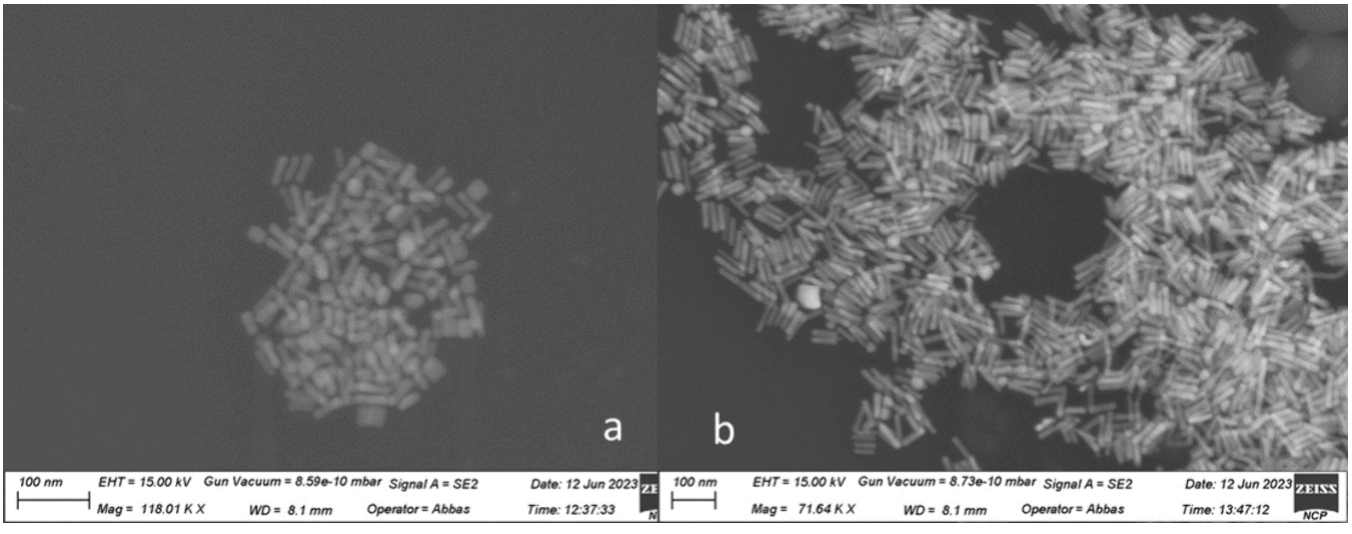

Figure 2. SEM images of AuNRs (a) without nitric acid and (b) with the maximum concentration of nitric acid.

https://doi.org/10.1021/acsomega.4c01313
ACS Omega 2024, 9, 33616−33628

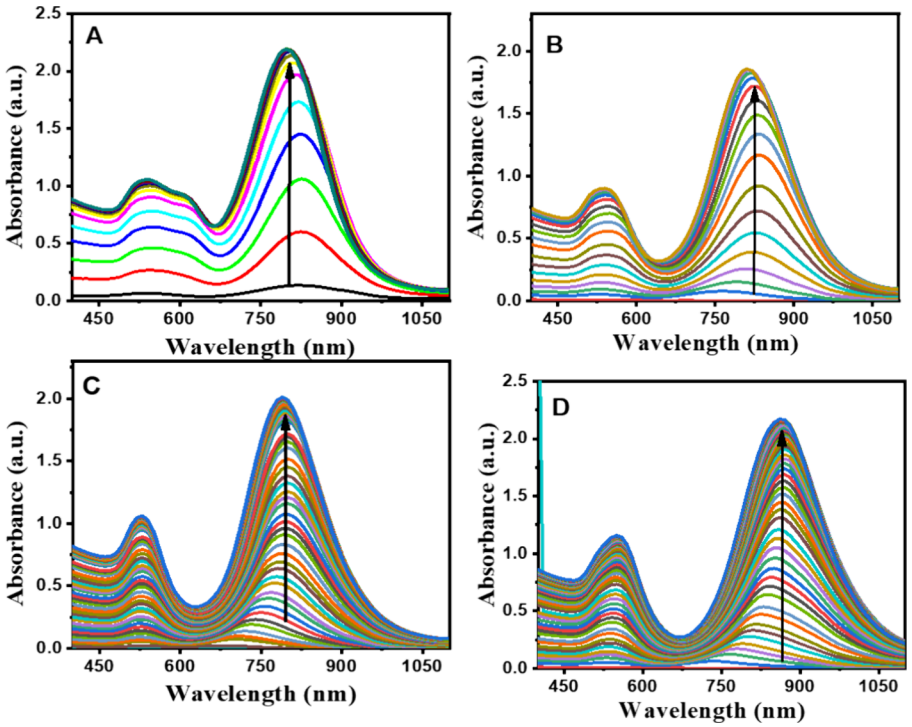

Figure 3. UV−vis spectra of growth solution after the addition of seeds. (A) RX_0 with no HNO_3, (B) RC_2 with 300 μL, (C) RB_3 with 500 μL, and (D) RD_5 with 1100 μL of HNO_3 in sample solution for growth times of 30, 60, 80, and 85 min, respectively. The arrow represents growth process.

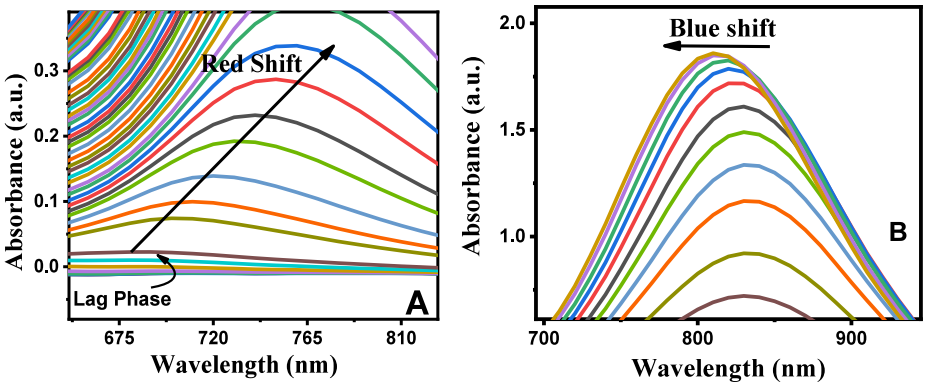

Figure 4. Representation of stages during the growth process. (A) The lag phase shows the start of the growth process on the seed nuclei, and the red shift shows the increase in the length of the nanorods. (B) Stabilization phase encountering the blue shift after the formation of nanorods of the respective aspect ratio.

where A_1 = initial absorbance value, A_2 = final absorbance value, x_0 = center, and dx = time constant. The reciprocal of the time constant, 1/dx, which is the maximum gradient of the sigmoidal curve, has been used as the rate of reaction. Kinetic parameters for the growth of gold nanorods were determined by fitting the maximum wavelength data with the nonlinear Boltzmann model.

3.6. Effect of Nitric Acid on AuNR Growth. It was observed that the reaction rates decreased as the concentration of HNO_3 was incremented. The apparent rate constants showed a linear dependence with the increment of HNO_3, as can be observed in Figure 6, having a range of growth rates from 0.34 to 0.12 for the lowest and highest molar ratios of HNO_3/Au^{3+}, respectively. It showed that with the increment of more acidic conditions, the growth of the gold nanorods became slow, leading to the deposition of the Au atoms along the longitudinal axis extending the nanorods in length. Thus, there is an enhancement in the aspect ratio of the gold nanorods with increasing HNO_3 concentration.

Briefly, synthesized small spherical gold nanoparticles were used as seeds for the fabrication of large-size nanorods. The mechanism followed a controlled route to avoid and inhibit the secondary nucleation. Acidic conditions decreased the transversal and longitudinal growth rates of gold nanorods. The LSPR showed a red shift with the increment of HNO_3 until a saturation point was attained. At the lower pH, the formation of AuNRs was slow at the beginning; however, reduction of a greater amount of gold atoms led to the red shift of LSPR and caused an upper longitudinal growth. The growth of nanorods was observed as a process with three stages: a quasi-isotropic seed growth, until seeds reached a critical size and the growth phase began. Then, optical density increased progressively and the LSPR underwent a red shift. After that, the stabilization phase took place, where the UV−vis spectrum showed a slight LSPR

https://doi.org/10.1021/acsomega.4c01313
ACS Omega 2024, 9, 33616−33628

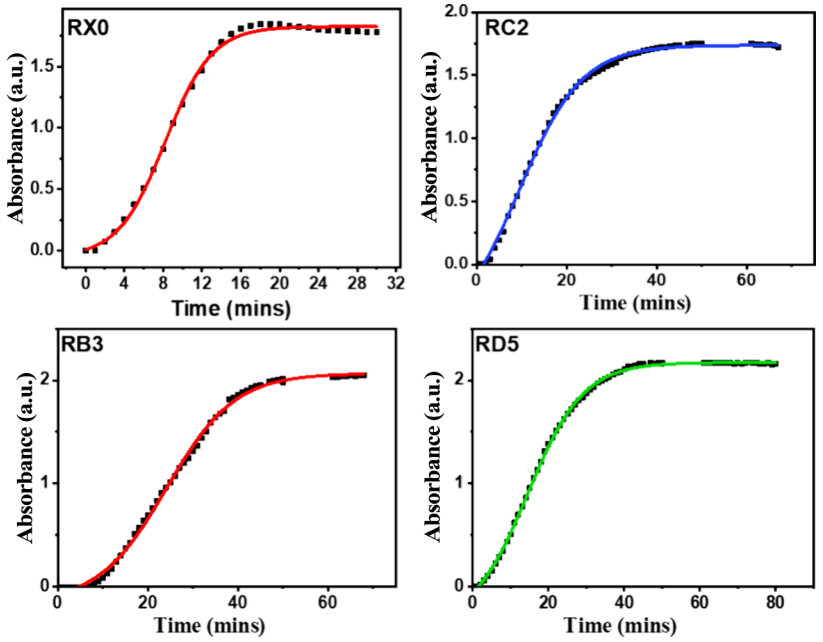

Figure 5. Absorbance of the longitudinal plasmon maximum wavelength as a function of time for RX_0, RC_2, RB_3, and RD_5, respectively (the solid line represents the Boltzmann fit of curves).

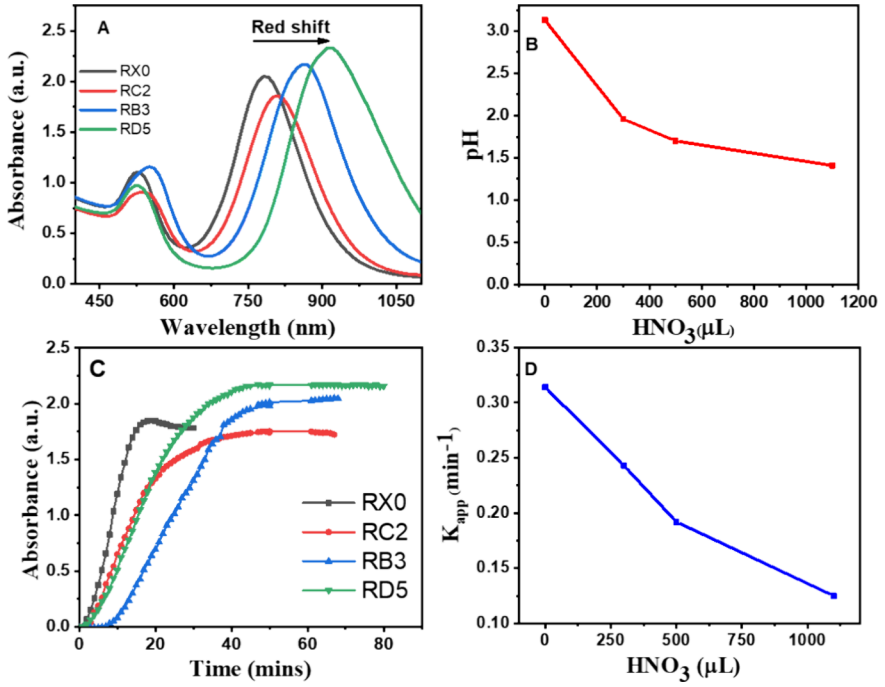

Figure 6. LSPR-dependent behavior of the gold nanorods during the growth process. (A) Red shift of localized surface plasmon resonance with increment of nitric acid conditions. (B) pH as a function of added nitric acid. (C) Absorbance of longitudinal plasmon maximum wavelength as a function of time. (D) Gold nanorods' apparent growth rate as a function of added nitric acid.

blue shift. To determine the apparent growth rates of the AuNRs, the experimental data was fitted with theoretical nonlinear Boltzmann function and normalized growth curves were obtained by plotting the absorbance against time. The analytical solution of the model was compared well with our experimental data and other data available in literature.[51−53]

3.7. UV−Visible Analysis of AuNRs@MWCNTs. Figure 7A shows the UV spectra of AuNRs incorporated into MWCNTs. MWCNTs showed the UV band at 220 nm. The SPR and LSPR bands of the AuNRs were at 525 and 910 nm, respectively. A well-defined hypsochromic or blue shift was observed for AuNR @MWCNTs, which confirmed the incorporation of AuNRs@MWCNTs. The SEM image of AuNRs@MWCNTs is displayed in Figure 7B. The image clearly showed the incorporation of gold nanorods on the surface of the MWCNTs.

3.8. Direct Optical Sensing of Glucose via UV−Visible Spectroscopy. Figure 8 displays the UV−visible spectra of Au nanorods in the presence of glucose. The linear range of glucose was kept from 0.1 to 28 mM. The Au nanorods showed two

https://doi.org/10.1021/acsomega.4c01313
ACS Omega 2024, 9, 33616−33628

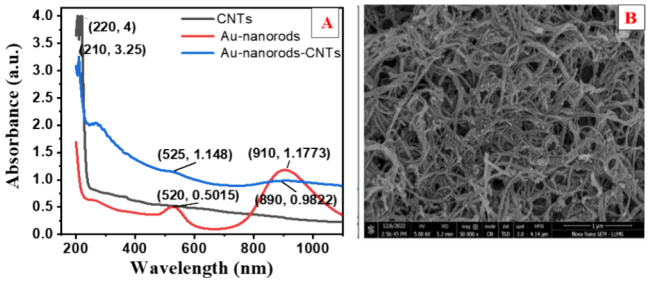

Figure 7. (A) UV−vis absorption spectra of MWCNTs alone, AuNRs, and AuNRs @MWCNT. (B) SEM image of AuNRs@MWCNTs.

absorption maxima at 510−530 and 690−930 nm for transverse and longitudinal axes, respectively. With the increment in glucose concentration, a gradual decrease in the transverse band at 510 nm and a hypochromic effect were observed in the longitudinal band, which led to gradual disappearance of the band.

The longitudinal plasmon band depicted a hypochromic shift at the respective lambda max of each sample corresponding to the aspect ratio of the AuNRs. The stability of the LSPR peak position indicated that the Au nanorods did not aggregate, possibly due to the stable interactions of Au with glucose concentrations used for this experiment. If the particles aggregate, then the LSPR band position will shift to a longer wavelength. The negative linear relationship between the glucose concentration and absorbance peak can be attributed to the nature of the interaction between the glucose molecules and nanoparticles. With the addition of glucose, the glucose molecules bonded to the surface of the gold nanorods. These results indicate that all the active available sites on gold nanorods were occupied by glucose, which infers that the synthesized anisotropic AuNRs have a higher sensitivity and they are more suitable for their versatile role in sensing application.[54] The mechanistic approach for sensing of glucose is illustrated in Figure 9.

Table 2 shows the performance of developed glucose sensors based on gold nanorods. The tabulated data presented in this work clearly showed that the sensitivity of AuNRs with high aspect ratio is higher than that of other nanorods. The observed higher sensitivity may correspond to high surface area in rods of high aspect ratio.

3.9. Electrochemical Sensing of Glucose via Gold Nanorods. *3.9.1. Stability Test.* Prior to nonenzymatic electrochemical sensing of glucose, the stability test of all the samples has been performed. All synthesized samples (supported and unsupported) maintained stability until 10 cycles and found to be stable at 100 mV s^{-1} in the potential window of +1 to −1 V in alkaline media at 25 °C. The synthesized samples maintained stability until 10 cycles. The graphs are placed in Supporting Information Figure S2.

3.9.2. Effect of Scan Rates on Modified GCEs in the Absence of Glucose. Figure 10 displays the CV response of GCE@$AuNRX_0$ and GCE@$AuNRX_0$@MWCNTs at different scan rates in 0.1 M NaOH at 25 °C. It is evident from the voltammograms that with the increase in scan rates, the peak current increased, which indicates that the diffusion rate increases as compared to the reaction rate according to the Randles−Sevcik equation.[18]

3.9.3. Nonenzymatic Glucose Sensing via AuNRs and AuNRs@MWCNT. Nonenzymatic glucose sensing was carried out in the presence of synthesized AuNR and AuNR @ MWCNT via CV. The AuNR-modified GC electrode was investigated in 0.1 M NaOH in the presence of different concentrations of glucose ranges from 5.5 μM to 0.33 mM at a scan rate of 50 mV s^{-1}. The voltammograms in Figure 11 inferred that with the increase in glucose concentrations, the

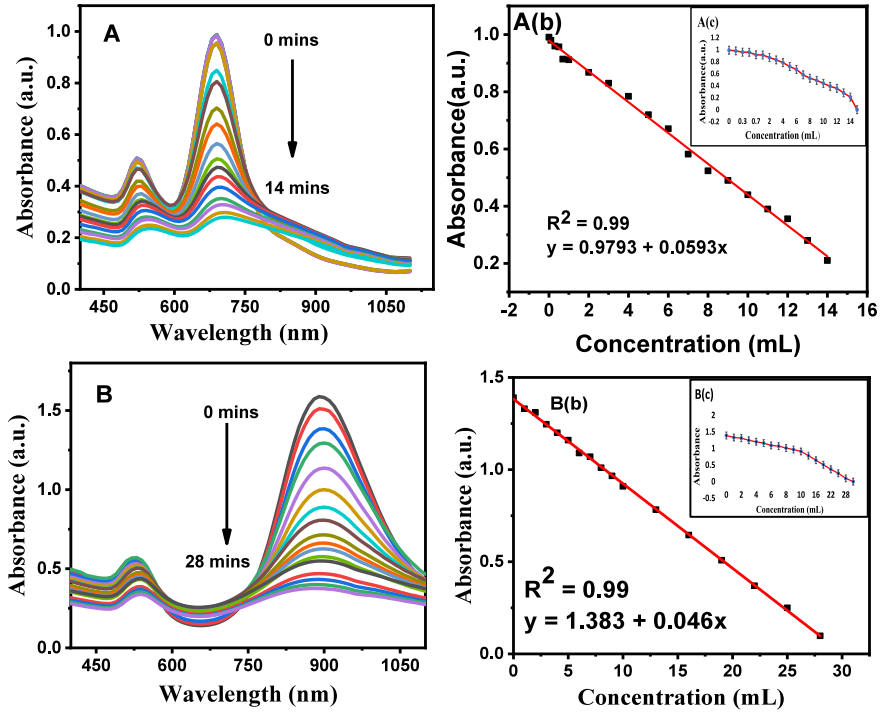

Figure 8. UV−visible absorption spectra of gold nanorods (A) RX_0 and (B) RD_5 mixed with different glucose concentrations ranging from 0.7 to 28 mM. A(b) and B(b) show the concentration profile versus absorbance of RX_0 and RD_5. A(c) and B(c) indicate error bars.

https://doi.org/10.1021/acsomega.4c01313
ACS Omega 2024, 9, 33616−33628

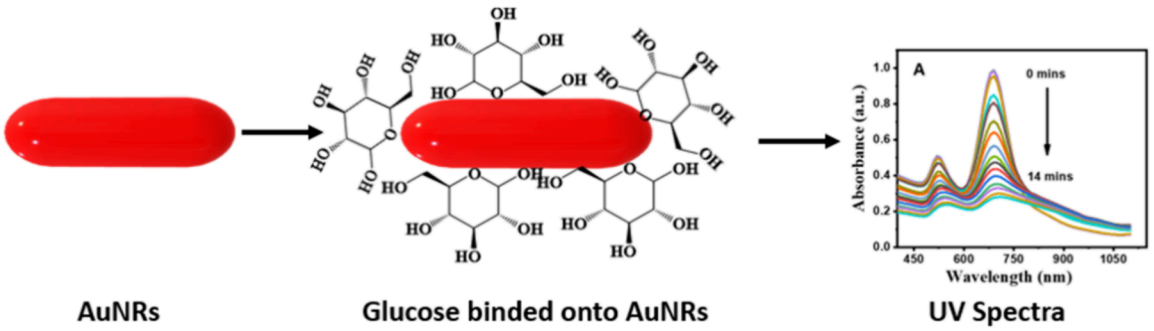

Figure 9. Representation of the mechanism of glucose sensing by gold nanorods.

Table 2. Optical Glucose Sensing with a Synthesized AuNR Sensor via UV-Visible Spectroscopy

sample	linear range	LOD (μM)	LOQ (μM)	sensitivity (μA mM^{-1}cm^{-2})
AuNRX$_0$	0.7−14 mM	57	174	53
AuNRD$_5$	1−28 mM	111	340	70

peak current increased. Glucose adsorption on the gold nanorod surface in NaOH occurred with the help of anomeric carbon. This led to the gluconolactone radical formation by dehydrogenation of adsorbed glucose. Later, the oxidation occurred via the reaction of gluconolactone with adsorbed OH^- ions. The increment in peak current led to the oxidation peak appearing in the anodic direction, which is assigned to the continuous oxidation of glucose.[18,30]

The structure of the GCE surface and the morphology of the adsorbed intermediates are very important for the oxidation of glucose. For successful glucose oxidation, the presence of a good number of active sites on the gold surface was very crucial. Here, AuOH acted as an available active site. When glucose is added to the system containing the AuNR-modified GC electrode in 0.1 M NaOH, several electrochemical processes occur, leading to the observed changes in the CV response. (1) Glucose adsorption on the gold nanorods' surface: Glucose molecules adsorb onto the surface of gold nanorods (AuNRs) due to the presence of anomeric carbon. This adsorption process is facilitated by the interaction between glucose molecules and the gold surface. (2) Dehydrogenation of adsorbed glucose: Once adsorbed, glucose molecules undergo dehydrogenation, leading to the formation of gluconolactone radicals. This step involves the removal of hydrogen atoms from the adsorbed glucose molecules. (3) Formation of gluconolactone: Gluconolactone is formed as an intermediate product in the dehydrogenation process. This molecule plays a crucial role in the subsequent oxidation reactions. (4) Oxidation of gluconolactone: In the presence of hydroxide ions (OH−) in solution, gluconolactone undergoes oxidation. This oxidation reaction involves the transfer of electrons, resulting in the conversion of gluconolactone to gluconic acid. (5) Increase in peak current: The oxidation of gluconolactone generates a current response in the cyclic voltammogram. As the concentration of glucose increases, more gluconolactone is produced, leading to an increase in the peak current observed in the CV response. (6) Continuous oxidation of glucose: The increment in the peak current corresponds to the continuous oxidation of glucose molecules present in the solution. This process occurs at the electrode surface and is detected through changes in the CV response.[55−57,18,30]

The said mechanism is sketched in Figure 12, and related equations are as follows:

$$\mathrm{Au} + \mathrm{OH}- \rightarrow \mathrm{Au(OH)}- \text{(basic medium)}$$

$$\mathrm{Au(OH)}- + \text{glucose} \rightarrow \text{glucolactone} + \mathrm{Au} + \mathrm{OH}- + \mathrm{H}+$$

$$\text{glucolactone} \rightarrow \text{gluconic acid(hydrolysis)}$$

3.9.4. Effect of Scan Rates. The effect of scan rates on the peak current in the presence of maximum glucose concentration was monitored (Figure 13). The voltammograms inferred that with the increase in scan rates, the peak current was increased as the concentration of adsorbed molecules of glucose at active

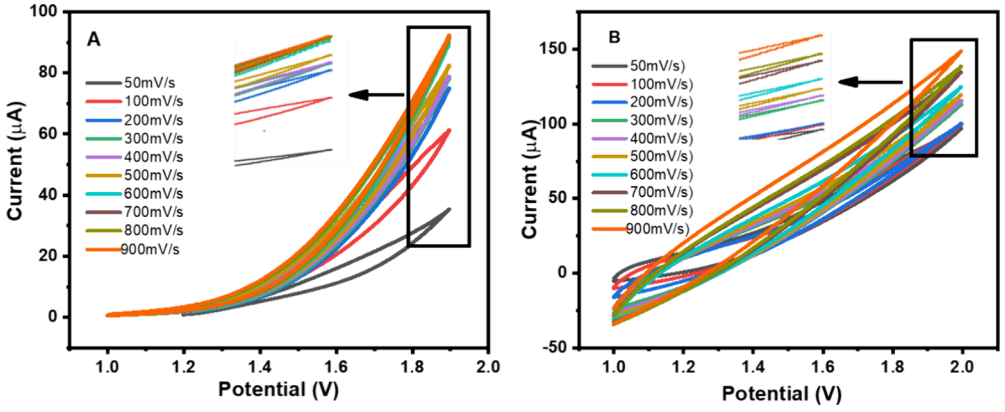

Figure 10. CV responses at different scan rates for (A) GCE@AuNRX$_0$ and (B) GCE@AuNRX$_0$@MWCNTs.

https://doi.org/10.1021/acsomega.4c01313
ACS Omega 2024, 9, 33616−33628

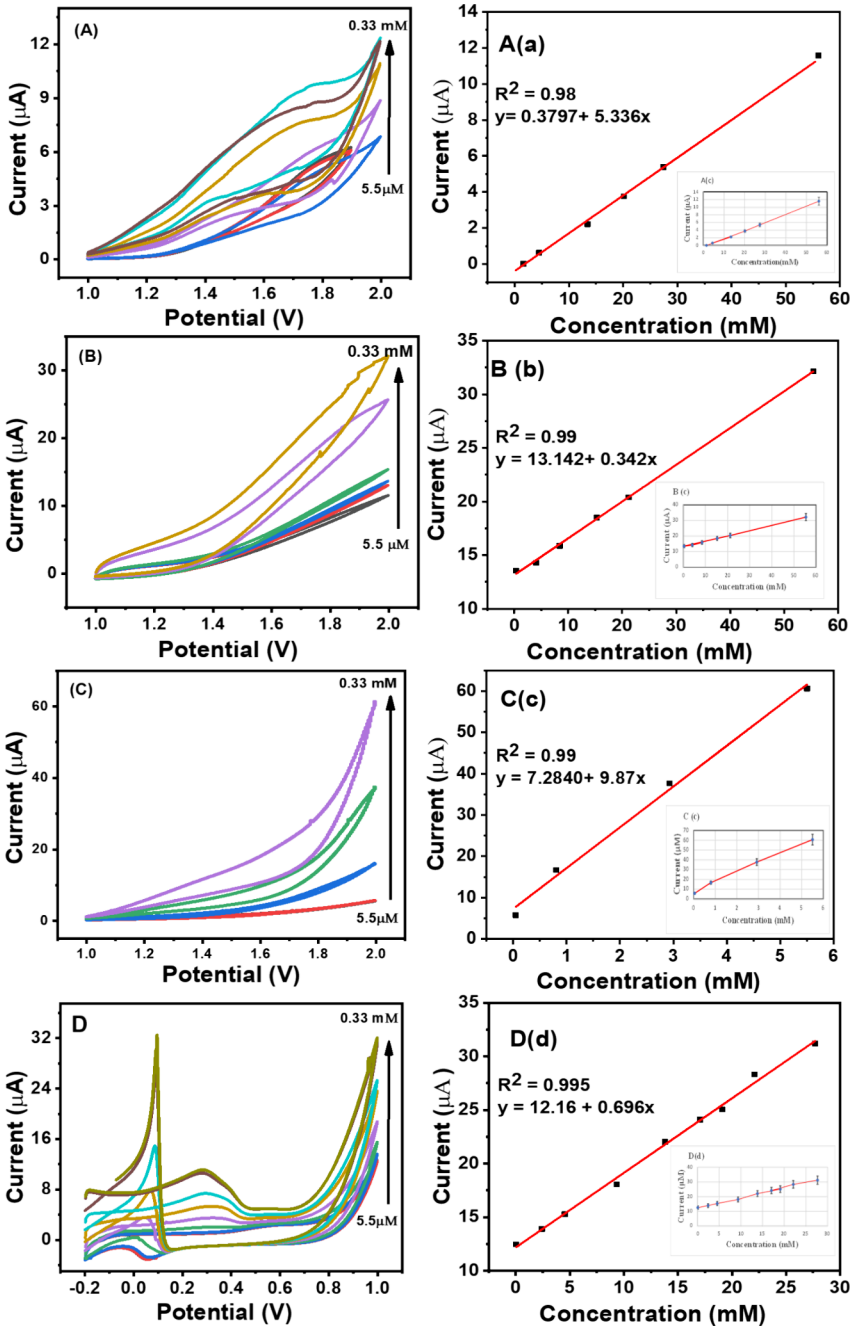

Figure 11. CV responses of (A) GCE@AuNRX$_0$, (B) GCE@AuNRX$_0$@MWCNTs, (C) GCE @AuNRD$_5$, and (D) GCE@AuNRD$_5$@MWCNTs for glucose sensing. Calibration curves of fabricated electrodes are represented in A(a), B(b), C(c), and D(d). Error bars are represented in inset of A(a), B(b), C(c), and D(d).

sites increased and conversion to glucolactone occurred.[30] The increment in the peak current led the oxidation peak to appear in the anodic direction, which is assigned to the continuous oxidation of glucose.

Table 3 shows the performances of fabricated glucose sensors based on AuNRs and AuNRs @MWCNTs modified onto the GCE surface. The comparative analysis showed that the sensitivity of AuNRX$_0$ @MWCNTs is higher than others, which may be due to availability of the high surface area (Table 4). The order of sensitivity was found to be AuNRX$_0$@MWCNTs > AuNRD$_5$@MWCNTs > AuNRD$_5$ > AuNRX$_0$. We observed that MWCNT-functionalized gold nanorods are promising candidates for glucose sensing.

The comparative analysis of our reported values with the literature is summarized in Table 4.

3.9.5. Reproducibility of the Fabricated Electrode System. Designed electrodes remained stable over multiple cycles of use as a biosensor. Overall efficiency decreased to 90% after five cycles. The figure is displayed in the Supporting Information, Figure S3.

CONCLUSIONS

Gold nanorods were successfully fabricated by employing a seed-mediated method. The aspect ratios of the gold nanorods were tuned by optimizing the concentration of HNO_3. SEM and UV results revealed the formation of nanorods of different

https://doi.org/10.1021/acsomega.4c01313
ACS Omega 2024, 9, 33616−33628

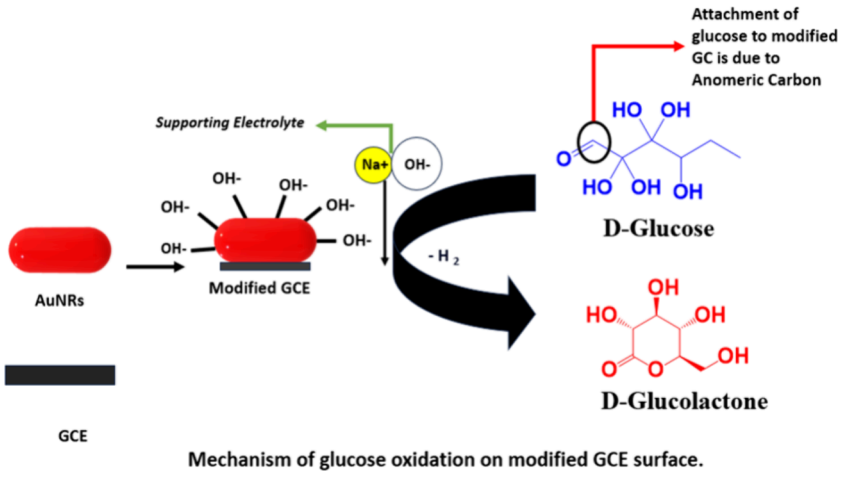

Figure 12. Illustration of the mechanism of electrochemical glucose sensing via gold nanorods.

Table 3. Glucose Sensing Characteristics of Fabricated Sensors@GCE via AuNRs and AuNRs @MWCNTs

sample	linear range	LOD (μM)	LOQ (μM)	sensitivity (μA mM^{-1} cm^{-2})
AuNRX$_0$	5 μM−0.33 mM	58	176	3198
AuNRD$_5$	5 μM−0.33 mM	35.5	108	3961
AuNRX$_0$@MWCNTs	5 μM−0.33 mM	90	275	6536
AuNRD$_5$@MWCNTs	5 μM−0.33 mM	250	761	4004

Table 4. Comparison of Analytical Performances of Nonenzymatic Glucose Sensors

electrodes	linear range	LOD (μM)	sensitivity (μA mM^{-1} cm^{-2})	references
Ag-nanoparticle-decorated organic functionalized multiwall carbon nanotubes/Au-electrode	1.3−1000 μM	0.03	1057	58
AuNR/GCE	0.5−2.5 mM	18	440	12
AuNR/GCE	5−160 μM	1.58	13.7	30
MWCNT−AuNano/GCE	0.1−25 mM	10.0	0.55 ± 0.03	59
PTFE/GOx/AuNPs/PANI/MWCNTs/GCE	0.0625−1.19 mM	0.19	29.17	60
AuNRX0/GCE	5 μM−0.33 mM	58	3198	this work
AuNRD5/GCE	5 μM−0.33 mM	35.5	3961	this work
AuNRX0@MWCNTs/GCE	5 μM−0.33 mM	90	6536	this work
AuNRD5@MWCNTs/GCE	5 μM−0.33 mM	250	4004	this work

aspect ratios. UV spectra inferred the longitudinal shift (red shift) in the samples with varying concentrations of nitric acid. The growth kinetics inferred that as growth time increases, the particle size increases. Acidic conditions decreased the transversal rate and increased the longitudinal growth rate, confirming the formation of gold nanorods (of different aspect ratios). The LSPR showed a red shift with the increment of HNO_3 until a saturation point is attained. The growth of nanorods completed in three stages: the lag phase that involves a quasi-isotropic seed growth, until seeds reached a critical size and the growth phase began. At this stage, the optical density increased progressively and the LSPR underwent a red shift followed by the stabilization phase, where the UV−vis spectrum showed a slight LSPR blue shift, and then a constant value of the absorbance intensity was observed. It was witnessed that approximately at 2 min, particles were formed of smaller size, but with passage of time particle growth was increased. Based on the experimental results, we proposed that pH affected the CTAB micelle's stability and reduced its adsorption ability on the gold surface, leading to different deposition dynamics of gold atoms onto the gold seeds and the morphology variation of the final products. The synthesized gold nanorods were functionalized with MWCNTs via a one-pot facile synthetic method. Sensing applications of glucose via synthesized materials were carried out optically and electrochemically. The optical observations inferred that the detection limit of glucose via gold nanorods was within 0.7−28 mM. For electrochemical glucose sensing, the GCE was modified with AuNRs and AuNRs@MWCNTs. These sensors detected glucose in the range of 5.5 μM−0.33 mM. The modified electrodes exhibited a very high sensitivity with a broad linear range. The sensitivity of AuNRX$_0$@MWCNTs was found higher in comparison to the others. The order of sensitivity was found as AuNRX$_0$@MWCNTs > AuNRD$_5$@MWCNTs > AuNRD$_5$ > AuNRX$_0$. All the reported sensors hold very high sensitivity performances and can be good sensors for glucose sensing.

■ ASSOCIATED CONTENT

Data Availability Statement

The data sets generated during and/or analyzed during the current study are available from the corresponding author on reasonable request.

https://doi.org/10.1021/acsomega.4c01313
ACS Omega 2024, 9, 33616−33628

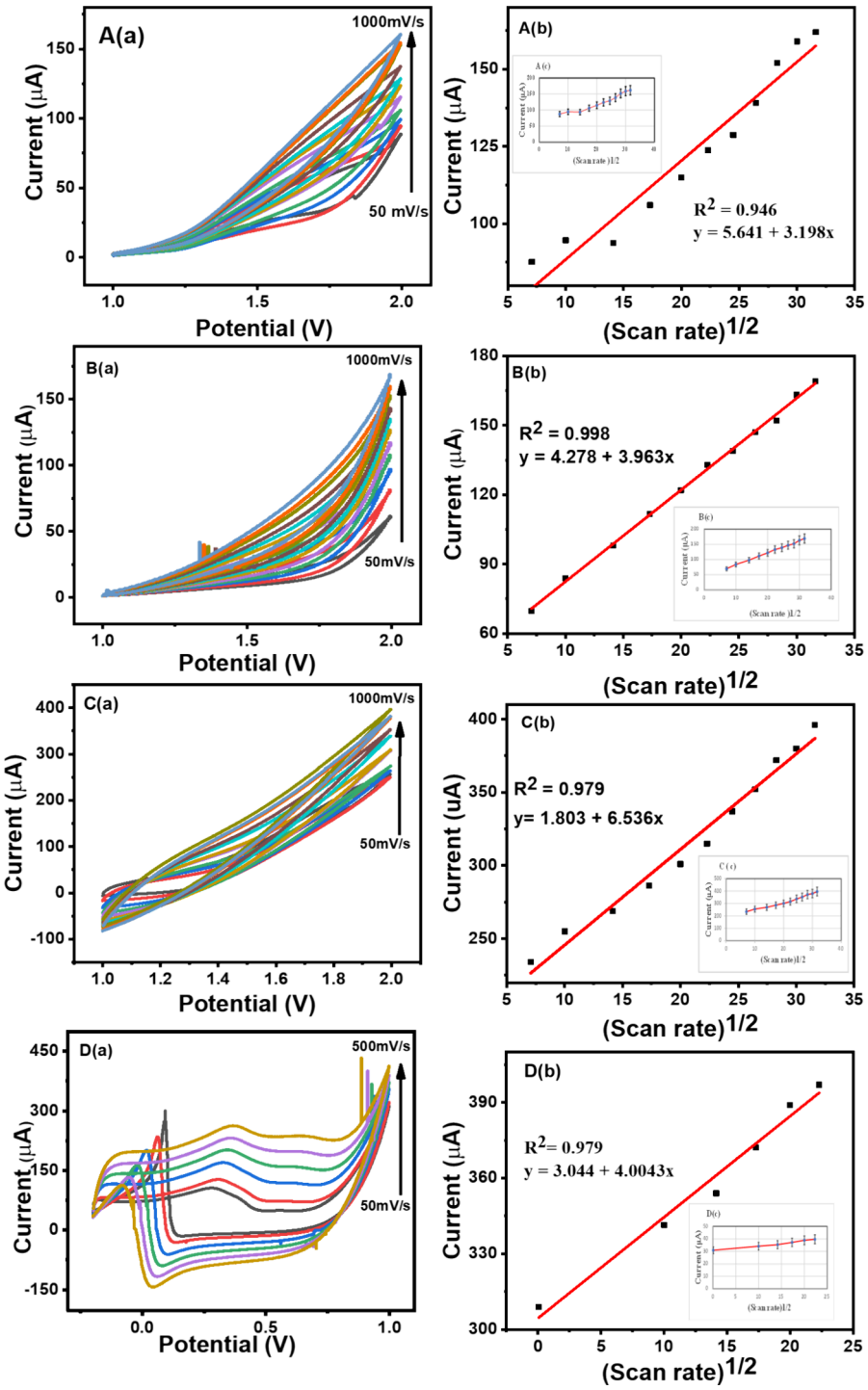

Figure 13. CV response at different scan rates in the presence of glucose: (A(a)) GCE@AuNRX$_0$, (B(a)) GCE@AuNRD$_5$, (C(a)) GCE@AuNRX$_0$@MWCNTs, and (D)a)) GCE@AuNRD$_5$@MWCNTs at different scan rates. Calibration curves (A(b)) GCE@AuNRX$_0$, (B(b)) GCE@AuNRD$_5$, (C(b)) GCE@AuNRX$_0$@MWCNTs, and (D(b)) GCE@AuNRD$_5$@MWCNTs at 50−1000 mVs^{-1}. Error bars are represented in insets of A(b), B(b), C(b), and D(b).

Supporting Information

The Supporting Information is available free of charge at https://pubs.acs.org/doi/10.1021/acsomega.4c01313.

Growth mechanism of gold nanorods; stability test for electrochemical sensing of glucose; and reproducibility of fabricated electrode system (PDF)

AUTHOR INFORMATION

Corresponding Author

Sana Sabahat − *Department of Chemistry, COMSATS University Islamabad, Islamabad 44000, Pakistan;* orcid.org/0000-0002-8787-3212; Phone: 0092-51-9049-5922; Email: s.sabahat@comsats.edu.pk

https://doi.org/10.1021/acsomega.4c01313
ACS Omega 2024, 9, 33616−33628

Authors

Yumna Nazish − *Department of Chemistry, COMSATS University Islamabad, Islamabad 44000, Pakistan*

Farhat Saira − *Nanoscience and Technology Division, National Centre for Physics (NCP), QAU Campus, Islamabad 44000, Pakistan*

Iqra Tariq − *Department of Chemistry, COMSATS University Islamabad, Islamabad 44000, Pakistan*

Zia Ul Haq Khan − *Department of Chemistry, COMSATS University Islamabad, Islamabad 44000, Pakistan*

Rahman Shah Zaib Saleem − *Department of Chemistry and Chemical Engineering, SBASSE, Lahore University of Management Sciences (LUMS), DHA, Lahore 54792, Pakistan;* orcid.org/0000-0002-9615-4471

Mahmood M. S. Abdullah − *Department of Chemistry, College of Science, King Saud University, Riyadh 11451, Saudi Arabia;* orcid.org/0000-0002-8057-8376

Yong-Mei Chen − *College of Chemistry, Beijing University of Chemical Technology, Beijing 100029, China;* orcid.org/0000-0003-1386-1574

Complete contact information is available at: https://pubs.acs.org/10.1021/acsomega.4c01313

Author Contributions

Conception, experimental design, manuscript composition, and supervision were done by S.S. Y.N. and I.T. did literature review, experimental work, and manuscript writing. F.S. helped in the conduction of electrochemical testing of synthesized materials. Z.U.H.K. helped in reviewing the draft. R.S.Z.S. helped in data curation. M.M.S.A. and Y.-M.C. helped in characterization and analysis.

Notes

The authors declare no competing financial interest.

■ ACKNOWLEDGMENTS

The authors acknowledge the financial support through Researchers Supporting Project number (RSPD2024R688), King Saud University, Riyadh, Saudi Arabia.

■ REFERENCES

(1) Sharma, V. K.; Filip, J.; Zboril, R.; Varma, R. S. Natural inorganic nanoparticles-formation, fate, and toxicity in the environment. *Chem. Soc. Rev.* **2015**, *44* (23), 8410−8423.

(2) Baig, N.; Kammakakam, I.; Falath, W. Nanomaterials: a review of synthesis methods, properties, recent progress, and challenges. *Mater. Adv.* **2021**, *2*, 1821−1871.

(3) Chen, X.; Zhao, D.; An, Y.; Shi, L.; Hou, W.; Chen, L. Catalytic properties of gold nanoparticles immobilized on the surfaces of nanocarriers. *J. Nanopart. Res.* **2010**, *12* (5), 1877−1887.

(4) Shi, Y.; Yang, R.; Yuet, P. K. Easy decoration of carbon nanotubes with well dispersed gold nanoparticles and the use of the material as an electrocatalyst. *Carbon* **2009**, *47* (4), 1146−1151.

(5) Chin, K. C.; et al. Gold and silver coated carbon nanotubes: An improved broad-band optical limiter. *Chem. Phys. Lett.* **2005**, *409* (1−3), 85−88.

(6) Pannopard, P.; Khongpracha, P.; Probst, M.; Limtrakul, J. Structure and electronic properties of 'DNA-gold-nanotube' systems: A quantum chemical analysis. *J. Mol. Graph Model.* **2008**, *26* (7), 1066−1075.

(7) Xin, F.; Li, L. Decoration of carbon nanotubes with silver nanoparticles for advanced CNT/polymer nanocomposites. *Compos. Part A Appl. Sci. Manuf.* **2011**, *42* (8), 961−967.

(8) Hou, X.; Wang, L.; Zhou, F.; Wang, F. High-density attachment of gold nanoparticles on functionalized multiwalled carbon nanotubes using ion exchange. *Carbon NY* **2009**, *47* (5), 1209−1213.

(9) Roach, L.; Coletta, P. L.; Critchley, K.; Evans, S. D. Controlling the Optical Properties of Gold Nanorods in One-Pot Syntheses. *J. Phys. Chem. C* **2022**, *126* (6), 3235−3243.

(10) Jana, N. R. *Colloidal Gold Nanorods: Science and Technology*. CRC Press 2023 1−152.

(11) Zheng, J.; Cheng, X.; Zhang, H.; Bai, X.; Ai, R.; Shao, L.; Wang, J. Gold nanorods: the most versatile plasmonic nanoparticles. *Chem. Rev.* **2021**, *121* (21), 13342−13453.

(12) Khalil, L.; Sabahat, S.; Ahmed, W. Effect of Aspect Ratio on the Catalytic Activities of Gold Nanorods. *Catal. Lett.* **2023**, 1018.

(13) Onaciu, A.; Braicu, C.; Zimta, A. A.; Moldovan, A.; Stiufiuc, R.; Buse, M.; Ciocan, C.; Buduru, S.; Berindan-Neagoe, I. Gold nanorods: From anisotropy to opportunity. An evolution update. *Nanomedicine* **2019**, *14* (9), 1203−1226.

(14) Liang, C.; Luan, J.; Wang, Z.; Jiang, Q.; Gupta, R.; Cao, S.; Liu, K. K.; Morrissey, J. J.; Kharasch, E. D.; Naik, R. R.; Singamaneni, S. Gold nanorod size-dependent fluorescence enhancement for ultrasensitive fluoroimmunoassays. *ACS Appl. Mater. Interfaces* **2021**, *13* (9), 11414−11423.

(15) He, S.; Pang, W.; Wu, X.; Yang, Y.; Li, W.; Qi, H.; Yang, K.; Duan, X.; Wang, Y. Bidirectional Regulation of Cell Mechanical Motion via a Gold Nanorods-Acoustic Streaming System. *ACS Nano* **2022**, *16* (5), 8427−8439.

(16) Roberts, A.; Mahari, S.; Gandhi, S. Signal enhancing gold nanorods (GNR) and antibody modified electrochemical nanosensor for ultrasensitive detection of Japanese Encephalitis Virus (JEV) secretory Non-Structural 1 (NS1) biomarker. *J. Electroanal. Chem.* **2022**, *919*, No. 116563.

(17) Du, Z.; Yu, T.; He, W.; Yurtsever, A.; Izquierdo, R.; Jafari, M.; Siaj, M.; Ma, D. Enhancing efficiency of nonfullerene organic solar cells via using polyelectrolyte-coated plasmonic gold nanorods as rear interfacial modifiers. *ACS Appl. Mater. Interfaces* **2022**, *14*, 16185−16196.

(18) Sabahat, S.; Ejaz, M.; Saira, F.; Saleem, Z. S. R.; Nazish, Y.; Khalil, L.; Naeem, A. Surface plasmon resonance based synthesis of gold nanorods for sensing applications. *Chem. Pap.* **2023**, *77*, 5901−5911.

(19) Meng, L.; Zhang, J.; Li, H.; Zhao, W.; Zhao, T. Preparation and progress in application of gold nanorods. *J. Nanomater.* **2019**, *2019*, 1−11.

(20) Cho, I. H.; Kim, D. H.; Park, S. Electrochemical biosensors: Perspective on functional nanomaterials for on-site analysis. *Biomater. Res.* **2020**, *24* (1), 1−12.

(21) Yang, Q.; Zhu, G.; Singh, L.; Wang, Y.; Singh, R.; Zhang, B.; Zhang, X.; Kumar, S. Highly sensitive and selective sensor probe using glucose oxidase/gold nanoparticles/graphene oxide functionalized tapered optical fiber structure for detection of glucose. *Optik* **2020**, *208* (1−10), No. 164536.

(22) Duc Chinh, V.; Speranza, G.; Migliaresi, C.; Van Chuc, N.; Minh Tan, V.; Phuong, N.-T. Synthesis of Gold Nanoparticles Decorated with Multiwalled Carbon Nanotubes (Au-MWCNTs) via Cysteaminium Chloride Functionalization. *Sci. Rep.* **2019**, *9* (1−9), 5667.

(23) Bahadur, J.; Sen, D.; Mazumder, S.; Parkash, J.; Sathiyamoorthy, D.; Venugopalan, R. Decoration of Carbon Nanotubes with Metal Nanoparticles by Wet Chemical Method: A Small-Angle Neutron Scattering Study. *J. Nanosci. Nanotechnol.* **2010**, *10*, 2963−2971.

(24) Tessonnier, J. P.; Ersen, O.; Weinberg, G.; Pham-Huu, C.; Su, D. S.; Schlögl, R. Selective Deposition of Metal Nanoparticles Inside or Outside Multiwalled Carbon Nanotubes. *ACS Nano* **2009**, *3*, 2081−2089.

(25) Lipińska, W.; Grochowska, K.; Siuzdak, K. Enzyme immobilization on gold nanoparticles for electrochemical glucose biosensors. *Nanomaterials* **2021**, *11*, 1156.

(26) Yu, Z.; Lou, R.; Pan, W.; Li, N.; Tang, B. Nanoenzymes in disease diagnosis and therapy. *Chem. Commun.* **2020**, *56* (99), 15513−15524.

(27) Wang, G.; He, X.; Wang, L.; Gu, A.; Huang, Y.; Fang, B.; Geng, B.; Zhang, X. Non-enzymatic electrochemical sensing of glucose. *Microchim. Acta* **2013**, *180*, 161−186.
(28) Chen, Q.; Liu, M.; Zhao, J.; Peng, X.; Chen, X.; Mi, N.; Yin, B.; Li, H.; Zhang, Y.; Yao, S. Water-dispersible silicon dots as a peroxidase mimetic for the highly-sensitive colorimetric detection of glucose. *Chem. Commun.* **2014**, *50*, 6771−6774.
(29) Sun, Y.; Li, P.; Zhu, Y.; Zhu, X.; Zhang, Y.; Liu, M.; Liu, Y. In situ growth of TiO2 nanowires on Ti3C2MXenes nanosheets as highly sensitive luminol electrochemiluminescent nanoplatform for glucose detection in fruits, sweat and serum samples. *Biosens. Bioelectron.* **2021**, *194* (15), No. 113600.
(30) Nazish, Y.; Sabahat, S.; Saleem, R. S. Z.; Saira, F.; Yaqub, A. Effect of nano-morphologies on catalysis and non-enzymatic glucose sensing. *J. Mater. Res.* **2023**, 649.
(31) Wu, Q.; Chen, H.; Fang, A.; Wu, X.; Liu, M.; Li, H.; Zhang, Y.; Yao, S. Universal Multifunctional Nanoplatform Based on Target-Induced in Situ Promoting Au Seeds Growth to Quench Fluorescence of Upconversion Nanoparticles. *ACS Sens.* **2017**, *2* (12), 1805−1813.
(32) Yi, Y.; Deng, J.; Zhang, Y.; Li, H.; Yao, S. Label-free Si quantum dots as photoluminescence probes for glucose detection. *Chem. Commun.* **2013**, *49*, 612−614.
(33) Huang, N.; Zhang, S.; Yang, L.; Liu, M.; Li, H.; Zhang, Y.; Yao, S. Multifunctional Electrochemical Platforms Based on the Michael Addition/Schiff Base Reaction of Polydopamine Modified Reduced Graphene Oxide: Construction and Application. *ACS Appl. Mater. Interfaces* **2015**, *7* (32), 17935−17946.
(34) Hassan, M. H.; Vyas, C.; Grieve, B.; Bartolo, P. Recent advances in enzymatic and non-enzymatic electrochemical glucose sensing. *Sensors* **2021**, *21* (14), 4672.
(35) Juska, V. B.; Pemble, M. E. A critical review of electrochemical glucose sensing: Evolution of biosensor platforms based on advanced nanosystems. *Sensors* **2020**, *20* (21), 6013.
(36) Jiang, P.; Wang, Y.; Zhao, L.; Ji, C.; Chen, D.; Nie, L. Applications of gold nanoparticles in non-optical biosensors. *Nanomaterials* **2018**, *8* (12), 977.
(37) Shahid, A.; Nazir, F.; Khan, M. J.; Sabahat, S.; Naeem, A. A concise overview of advancements in ultrasensitive biosensor development. *Front. Bioeng. Biotechnol.* **2023**, *11*, No. 1288049, DOI: 10.3389/fbioe.2023.1288049.
(38) Sabahat, S.; Janjua, N. K.; Brust, M.; Akhter, Z. Electrochemical fabrication of self-assembled monolayer using ferrocene-functionalized gold nanoparticles on glassy carbon electrode. *Electrochim. Acta* **2011**, *56*, 7092−7096.
(39) Karimian, N.; Ugo, P. Recent advances in sensing and biosensing with arrays of nanoelectrodes. *Current Opinion in Electrochemistry* **2019**, *16*, 106−116.
(40) Albusta, N.; Alarabi, D.; Alsoud, S. A.; Keogh, M.; Akhtar, S.; Henari, F. Detection of glucose using gold nanoparticles prepared by green synthesis. *Int. J. Eng. Sci. Res.* **2018**, *6* (10), 1−11.
(41) Wei, M. Z.; Deng, T. S.; Zhang, Q.; Cheng, Z.; Li, S. Seed-mediated synthesis of gold nanorods at low concentrations of CTAB. *ACS Omega* **2021**, *6* (13), 9188−9195.
(42) Busbee, B. D.; Obare, S. O.; Murphy, C. J. An Improved Synthesis of High-Aspect-Ratio Gold Nanorods. *Adv. Mater.* **2003**, *15*, 414−416.
(43) Jana, N. R.; Gearheart, L.; Murphy, C. J. Seed-Mediated Growth Approach for Shape-Controlled Synthesis of Spheroidal and Rod-like Gold Nanoparticles Using a Surfactant Template. *Adv. Mater.* **2001**, *13* (18), 1389−1393.
(44) Altansukh, B.; Yao, J.; Wang, D. Synthesis and Characterization of Gold Nanorods by a Seeding Growth Method. *J. Nanosci. Nanotechnol.* **2008**, *8*, 1−4.
(45) Murphy, C. J.; Sau, T. K.; Gole, A. M.; Orendorff, C. J.; Gao, J.; Gou, L.; Hunyadi, S. E.; Li, T. Anisotropic metal nanoparticles: Synthesis, assembly, and optical applications. *J. Phys. Chem. B* **2005**, *109* (29), 13857−13870.
(46) Yong, K. T.; Sahoo, Y.; Swihart, M. T.; Schneeberger, P. M.; Prasad, P. N. Templated synthesis of gold nanorods (NRs): The effects of cosurfactants and electrolytes on the shape and optical properties. *Top. Catal.* **2008**, *47* (1−2), 49−60.
(47) Abdullah, A.; Altaf, M.; Khan, H. I.; Khan, G. A.; Khan, W.; Ali, A.; Bhatti, A. S.; Khan, S. U.; Ahmed, W. Facile room temperature synthesis of multifunctional CTAB coated gold nanoparticles. *Chem. Phys.* **2018**, *510*, 30−36.
(48) Wu, H. Y.; Chu, H. C.; Kuo, T. J.; Kuo, C. L.; Huang, M. H. Seed-mediated synthesis of high aspect ratio gold nanorods with nitric acid. *Chem. Mater.* **2005**, *17* (25), 6447−6451.
(49) Park, K.; Drummy, L. F.; Wadams, R. C.; Koerner, H.; Nepal, D.; Fabris, L.; Vaia, R. A. Growth mechanism of gold nanorods. *Chem. Mater.* **2013**, *25* (4), 555−563.
(50) Sahu, A. K.; Das, A.; Ghosh, A.; Raj, S. Understanding blue shift of the longitudinal surface plasmon resonance during growth of gold nanorods. *Nano Express* **2021**, *2* (1), No. 010009.
(51) Bullen, C.; Zijlstra, P.; Bakker, E.; Gu, M.; Raston, C. Chemical kinetics of gold nanorod growth in aqueous CTAB solutions. *Cryst. Grow. Des.* **2011**, *11* (8), 3375−3380.
(52) Almada, M.; Ruiz, E. D.; Ibarra-Hurtado, J.; Hassan, N.; Kogan, M. J.; Cadena-Nava, R. D.; Valdés, M. A.; Juárez, J. Growth kinetics of gold nanorods synthesized by a seed-mediated method under pH acidic conditions. *J. Nanosci. Nanotechnol.* **2016**, *16* (7), 7707−7714.
(53) Hepel, M.; Blake, D.; McCabe, M.; Stobiecka, M.; Coopersmith, K.Assembly of gold nanoparticles induced by metal ions. In *Functional Nanoparticles for Bioanalysis, Nanomedicine, and Bioelectronic Devices* American Chemical Society 2012, *1*, 207 240.
(54) Ren, X.; Yang, L.; Ren, J.; et al. Direct Interaction Between Gold Nanorods and Glucose. *Nanoscale Res. Lett.* **2010**, *5*, 1658.
(55) Chen, Q.; et al. Water-dispersible silicon dots as a peroxidase mimetic for the highly-sensitive colorimetric detection of glucose. *Chem. Commun.* **2014**, *50* (51), 6771−6774.
(56) Yi, Y.; Deng, J.; Zhang, Y.; Li, H.; Yao, S. Label-free Si quantum dots as photoluminescence probes for glucose detection. *Chem. Commun.* **2013**, *49* (6), 612−614.
(57) Sun, Y.; Li, P.; Zhu, Y.; Zhu, X.; Zhang, Y.; Liu, M.; Liu, Y. In situ growth of TiO_2 nanowires on Ti3C2MXenes nanosheets as highly sensitive luminol electrochemiluminescent nanoplatform for glucose detection in fruits, sweat and serum samples. *Biosen. Bioelectro.* **2021**, *194*, No. 113600.
(58) Ensafi, A. A.; Zandi-Atashbar, N.; Rezaei, B.; Ghiaci, M.; Chermahini, M. E.; Moshiri, P. Non-enzymatic glucose electrochemical sensor based on silver nanoparticle decorated organic functionalized multiwall carbon nanotubes. *RSC Adv.* **2016**, *6* (65), 60926−60932.
(59) Branagan, D.; Breslin, C. B. Electrochemical detection of glucose at physiological pH using gold nanoparticles deposited on carbon nanotubes. *Sensors Actuators, B Chem.* **2019**, *282*, 490−499.
(60) Zeng, X.; Zhang, Y.; Du, X.; Li, Y.; Tang, W. A highly sensitive glucose sensor based on a gold nanoparticles/polyaniline/multi-walled carbon nanotubes composite modified glassy carbon electrode. *New J. Chem.* **2018**, *42* (14), 11944−11953.

https://doi.org/10.1021/acsomega.4c01313
ACS Omega 2024, 9, 33616−33628